Available online at www.sciencedirect.com
ScienceDirect
Bioorganic & Medicinal Chemistry 14 (2006) 6962–6970
Bioorganic & Medicinal Chemistry

Acenaphtho[1,2-*b*]pyrrole derivatives as new family of intercalators: Various DNA binding geometry and interesting antitumor capacity

Zhichao Zhang,[a] Yuanyuan Yang,[b] Danni Zhang,[a] Yuanyuan Wang,[a] Xuhong Qian[a,c,*] and Fengyu Liu[d,*]

[a]*State Key Laboratory of Fine Chemicals, Dalian University of Technology, Dalian 116012, China*
[b]*School of Environmental and Biological science and Technology, Dalian University of Technology, Dalian 116024, China*
[c]*Shanghai Key Laboratory of Chemical Biology, East China University of Science and Technology, Shanghai 200237, China*
[d]*Chemistry department of Dalian University of Technology, Dalian 116012, China*

Received 12 May 2006; revised 15 June 2006; accepted 16 June 2006
Available online 7 July 2006

Abstract—A series of acenaphtho[1,2-*b*]pyrrole derivatives were synthesized and their intercalation geometries with DNA and antitumor activities were investigated in detail. From combination of SYBR Green–DNA melt curve, fluorescence titration, absorption titration, and circular dichroism (CD) studies, it was identified that to different extent, all the compounds behaved as DNA intercalators and transformed B form DNA to A-like conformation. The different intercalation modes for the compounds were revealed. The compounds containing a methylpiperazine substitution (series **I**) intercalated in a fashion that the long axis of the molecule paralleled to the base-pair long axis, while the alkylamine- substituted compounds (series **II** and **III**) located vertically to the long axis of DNA base pairs. Consequently, the DNA binding affinity of these compounds was obtained with the order of **II** > **III** > **I**, which attributed to the role of the substitution in binding geometry. Further, cell-based studies showed all the compounds exhibited outstanding antitumor activities against two human tumor cell lines with IC_{50} ranging from 10^{-7} to 10^{-6} M. Interestingly, compound ^{1}**a** (a compound in series **I**), whose binding affinity was one of the lowest but altered DNA conformation most significantly, showed much lower IC_{50} value than other compounds. Moreover, it could induce tumor cells apoptosis, while the compounds ^{2}**a** and ^{3}**a** (in series **II** and **III**, respectively) could only necrotize tumor cells. Their different mechanism of killing tumor cells might lie in their different DNA binding geometry. It could be concluded that the geometry of intercalator–DNA complex contributed much more to the antitumor property than binding affinity.

1. Introduction

There is substantial and continuing interest in artificial molecules that bind and interact with DNA. Most of these molecules have been studied with the purpose of developing novel antitumor lead compound.[1–3] Studies on the binding geometry of various ligands to DNA have revealed that the biological activity correlated with not only their DNA binding affinity, but also the binding mode.[4,5] For example, Viola G. found the more efficiency of DNA cleavage of externally bound dye compared with the intercalated one.[6] Cholody W. M. demonstrated that the best model to account for the excellent antitumor property of BIAs involved the intercalation of one chromophore while the other resided in the minor groove.[7,8] So, understanding the nature of binding geometry of ligand–DNA complex may contribute to the design of more efficient antitumor leads.

The heterocyclic molecules containing a flat, generally π-deficient aromatic system form a famous class of antitumor agents.[9–12] They could bind to DNA by intercalation between base pairs of the double helix. Recently, we reported a series of electron-deficient acenaphtho-heterocyclic compounds as novel antitumor leads,[13,14] 8-oxo-8*H*-acenaphtho[1,2-*b*] pyrrole-9-carbonitrile and its derivatives. Combining the results of gel-shift studies and binding mode studies, it was illustrated that the different binding mode of these compound to DNA owing

Keywords: Antitumor agents; DNA; Intercalation; Geometry.
* Corresponding authors. E-mail addresses: xhqian@ecust.edu.cn; annyuer_liu@163.com

0968-0896/$ - see front matter © 2006 Elsevier Ltd. All rights reserved.
doi:10.1016/j.bmc.2006.06.029

to their different side chain rendered them different antitumor potency. These results offered us a promising platform to design novel antitumor lead compound. In addition, it promoted us to gain insight into the key structural features that account for binding geometry and consequently the antitumor potency, and the possible relationship between the binding mode of ligand–DNA and its antitumor property.

To this end, we further synthesized nine derivatives characterized by various substitutions with different length, flexibility, and π-deficiency. The binding geometry of these compounds to DNA was investigated by means of molecular spectra, and cell-based assay was performed to evaluate their antitumor properties. Through the SAR (structure–activity relationship) studies, we expected to find the constituent for more efficient biological and medical application.

2. Results and discussion

2.1. Synthesis and spectra

The structures of the new compounds are shown in Scheme 1. They were divided into three series **I**, **II**, and **III** according to methylpiperazine, dimethylethane, and dimethylpropane side chain. Spectral data of them were measured and are summarized in Table 1.

2.2. Binding affinity

The intercalation of the nine compounds to CT DNA was evaluated by SYBR Green–DNA melt curve. SYBR Green could intercalate all double-stranded DNA. Its self-fluorescence intensity is very weak but increases greatly when intercalates into DNA.[15,16] Figure 1 (curve ■) shows as the temperature increased from 45–95 °C and CT DNA became single-stranded, the fluorescence signal decreased due to the SYBR Green molecules released. When the nine compounds were added to the SYBR Green–DNA complexes, different fluorescence curves were exhibited due to their different binding affinity with DNA. The obtained flat curves strongly indicated the seven compounds (**^{1}a**, **^{2}a**, **^{2}b**, **^{2}c**, **^{3}a**, **^{3}b**, and **^{3}c**) competed with all of the SYBR Green molecules for the intercalation sites. Obviously, their DNA-intercalating properties were stronger than the typical intercalator–SYBR Green. The much weaker and the weakest competition were observed for **^{1}b** and **^{1}c**, respectively. The results proved the binding strength variations among these compounds.

Table 1. The spectral characteristics of the nine compounds in Tris–HCl buffer (pH 7.0)

Compound	Log ε	Absorption λ_{max} (nm)	Emission λ_{max} (nm)	Stock shift (nm)
^{1}a	3.417	590	603	13
^{2}a	3.073	603	613	10
^{3}a	2.857	602	613	11
^{1}b	3.546	570	587	17
^{2}b	3.220	593	608	15
^{3}b	3.167	592	608	16
^{1}c	3.302	572	589	15
^{2}c	3.141	594	610	16
^{3}c	3.082	594	611	17

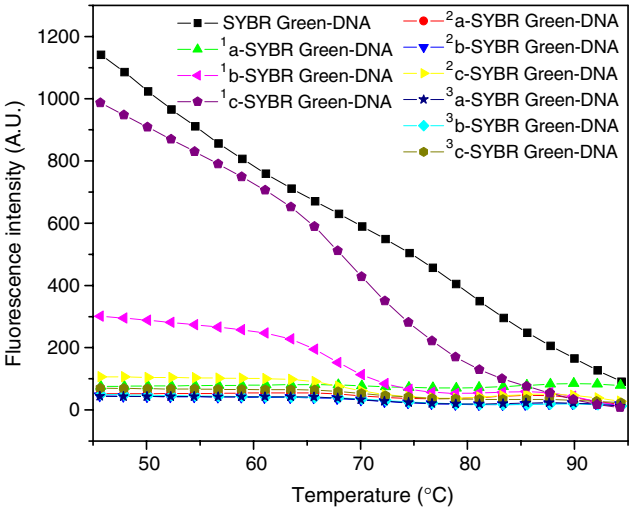

Figure 1. The effect of the nine compounds on the melt curve of SYBR Green–DNA complexes.

To identify the binding affinity to DNA, the Scatchard binding constants of the nine compounds were determined through fluorescence titration. The fluorescence

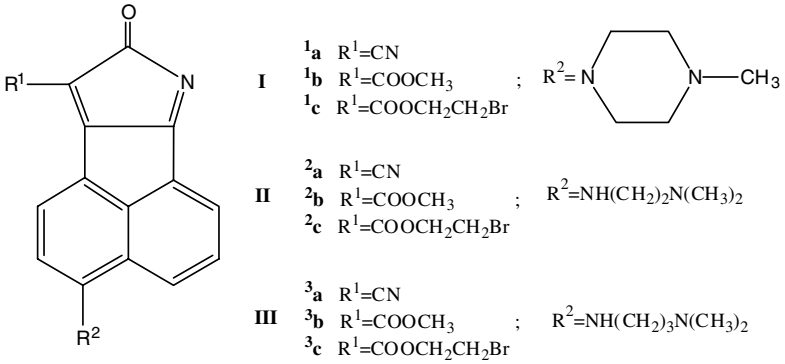

Scheme 1. Structure of some acenaphtho[1, 2-*b*]pyrrole derivatives.

of these compounds was quenched upon addition of CT DNA. The binding constants K_b were calculated (Fig. 2) and are summarized in Table 2 with the order of series **II** > **III** > **I**. The compounds of series **I** containing methylpiperazine substitution exhibited weaker affinity to DNA, while the much higher affinity was observed for alkylamine-substituted compounds of series **I** and **III**. These results were in good agreement with the SYBR Green–DNA melt curve experiment. In addition, the DNA affinity decreased in the order, CN > $COOCH_3$ > $COOCH_2CH_2Br$-introduced compounds. The stacking of π-bond interactions between the electron-deficient chromophore and the electron-rich purine–pyrimidine base plays an important role on DNA binding affinity.[10–12,17] As anticipated, the higher affinity was found for CN-introduced compounds, because the strongly electron-withdrawing moiety of the CN group led to higher electron-deficiency of planar ring system. Although $COOCH_2CH_2Br$ group was characteristic of stronger electron-withdrawing than $COOCH_3$ owing to the bromine atom, the lower DNA affinity was found for the former one. The more steric hindrance of larger moiety-$COOCH_2CH_2Br$ appeared to be responsible for it.

Another crucial structural feature for DNA binding affinity of intercalators is the properties of side chain on naphthalene moiety, such as the length and rigidity.[17–19] The data in Table 2 clearly indicated the weaker affinity for series **III** than **II**, which was much likely owing to the longer length of the substitution that sterically hindered the intercalation of the chromophore into the DNA base pairs. Similarly, the steric hindrance of semi-rigid methylpiperazine substitution resulted in the weakest affinity of series **I**.

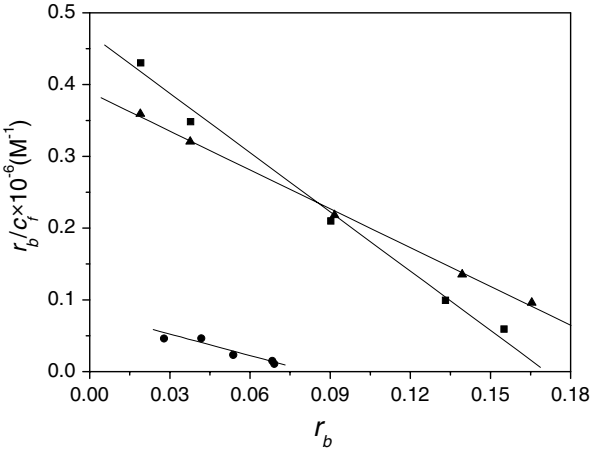

Figure 2. Scatchard plots of the binding of ^{1}**a** (●), ^{2}**a** (■), and ^{3}**a** (▲) with CT DNA in Tris–HCl buffer (pH 7.0). The compound concentration was 1, 2, 5, 8, and 10 μM, while the DNA concentration was kept as 50 μM.

Table 2. The DNA binding affinities and site densities for the nine compounds

Compound	$K_b \times 10^6$ (M^{-1})	n (Sites per base)	R^2
^{1}**a**	0.813 ± 0.035	0.084 ± 0.002	0.997
^{1}**b**	0.458 ± 0.011	0.010 ± 0.002	0.999
^{1}**c**	0.035 ± 0.003	0.050 ± 0.001	0.991
^{2}**a**	2.753 ± 0.292	0.171 ± 0.011	0.983
^{2}**b**	1.930 ± 0.349	0.302 ± 0.025	0.984
^{3}**b**	1.782 ± 0.221	0.285 ± 0.014	0.978
^{3}**a**	1.803 ± 0.043	0.216 ± 0.002	0.999
^{3}**b**	1.690 ± 0.195	0.286 ± 0.016	0.993
^{3}**c**	1.555 ± 0.163	0.305 ± 0.013	0.989

The n (apparent number of independent binding sites of DNA) values were also calculated by Scatchard analysis, as shown in Table 2. The n varied remarkably among the three series, much likely due to the difference in their chemical structure. The very small n of series **I** are consistent with their poor binding affinities.

2.3. Absorption titration

To further investigate the DNA binding mode of the three series of compounds to DNA and understand if the two kinds of substitution, methylpiperazine and alkylamine, played a different role in the process of binding to DNA, the compounds ^{1}**a**, ^{2}**a**, and ^{3}**a** were selected to perform the titration absorption spectra by CT DNA due to their highest binding affinity in each series (Fig. 3). In the case of compound ^{1}**a**, addition of DNA induced hypochromicity (32%) and a small red shift of the absorption maximum (2 nm) in the UV–vis spectra. A significantly difference and unusual phenomenon, however, was obtained for compounds ^{2}**a** and ^{3}**a**. Two bands were observed for the complexes. At low DNA/compound ratio, hypochromicity was found for the two bands. As the DNA concentration was increased, the spectra for the longer band showed pronounced hyperchromicity and bathochromic shift. The maximum bathochromic shifted about 12 and 16 nm as compared with that of the free ^{2}**a** and ^{3}**a**, respectively. The hypochromicity of the shorter band continued.

The distinguishable results of the spectrophotometric titration for series **I** and **II** or **III** could be interpreted as the existence of the different binding mode between the compounds containing methylpiperazine and alkylamine substitution. Significant hypochromicity and a slight red shift phenomenon exhibited in ^{1}**a**–DNA complex revealed a classical intercalation of ^{1}**a**–DNA.[20,21] While the absorption spectra of ^{2}**a** and ^{3}**a** recorded during the increase of DNA concentration could infer that two-step binding process occurred.[13] The first step occurred at low DNA/compound ratio, which spectra might attribute to the complexation and stacking of the compounds along DNA surface. This cooperative binding originated from intercalation and electrostatic attraction of the positively charged substitution and the negatively charged phosphate groups of DNA.[22] The second step occurred at high DNA/compound ratio, which spectra reflected the formation of a complete intercalation mode. In summary, their DNA intercalation geometry was very different from that of ^{1}**a**. It is reasonable to infer the stacking of series **II** and **III** was driven by the flexibility of the alkylamine substitution.

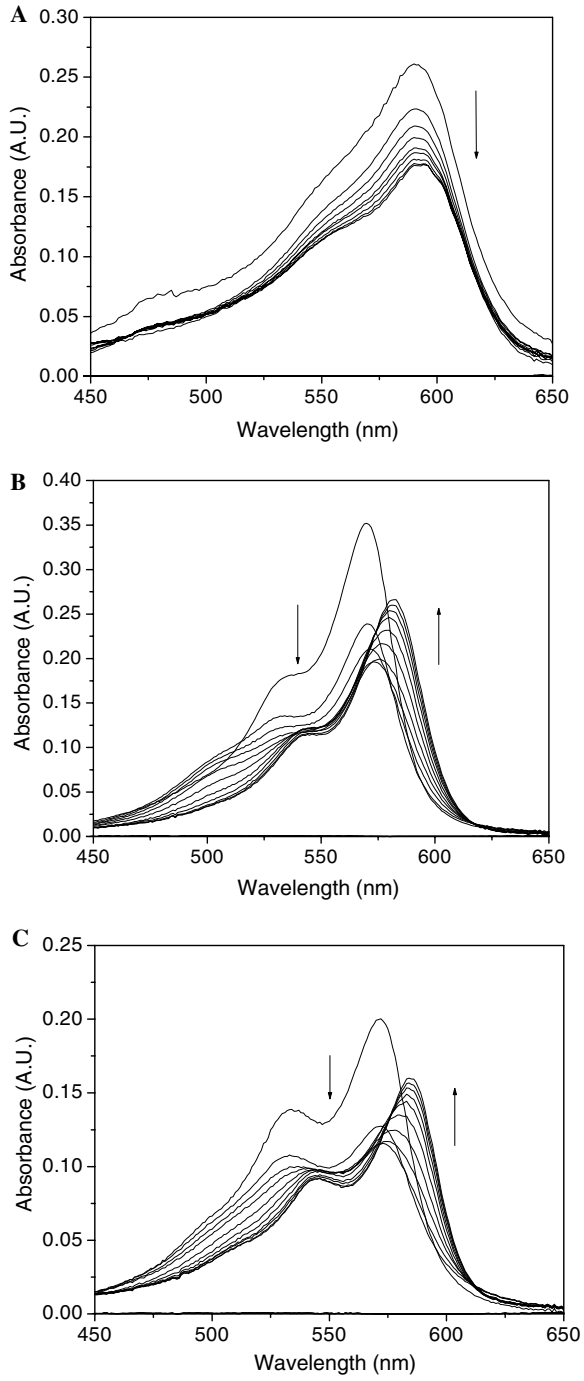

Figure 3. Spectrophotometric titrations of compounds **^{1}a** (A), **^{2}a** (B), and **^{3}a** (C) with CT DNA in Tris–HCl buffer (pH 7.0). The titration absorption spectra of compound by CT DNA were measured by keeping the compound concentration as 10 μM and varying the DNA concentration from 5 to 50 μM at 5 μM intervals.

2.4. Induced circular dichroism

To further distinguish the intercalation geometry of series **I** and **II** or **III**, circular dichroism spectra were performed and the role of the two kinds of substitutions in binding geometry to DNA was investigated. To illustrate how the compound located in the intercalation pocket, the induced circular dichroism (ICD) of **^{1}a**, **^{2}a**, and **^{3}a** was performed at DNA/compound ratio of 10, where all the compounds showed intercalative mode. According to experiments and theoretical studies, an intercalated chromophore centered near the helix axis of DNA should exhibit negative ICD for all long-wavelength transitions polarized parallel to the long axis of the base-pair pocket, while transitions perpendicular to this direction, but still in the plane of the nucleobases (i.e., parallel to the pseudo-dyad axis), should give positive ICD.[23–26] As shown in Figure 4, when CT DNA was added, a negative ICD signal was observed for **^{1}a** which contained a methylpiperazine substitution, suggesting that **^{1}a** intercalated into DNA with its long axis parallel to the base-pair long axis. On the contrary, the two alkylamine-substituted compounds **^{2}a** and **^{3}a** exhibited positive ICD signals. It indicated a vertical orientation in the intercalation pocket (Fig. 5). The different ICD signals additionally supported the notion that the compound **^{1}a** and **^{2}a** or **^{3}a** intercalated into DNA in different fashion. So far, the binding affinities of the three series of compounds could be explained further. In the case of series **II** and **III**, because chromophore intercalated into DNA in the way that long axis of the molecule perpendicularly oriented to the base-pair long axis, the alkylamine group exposed on DNA surface. By contrast, due to the parallel orientation of series **I** in DNA base-pair pocket, the semirigid methylpiperazine

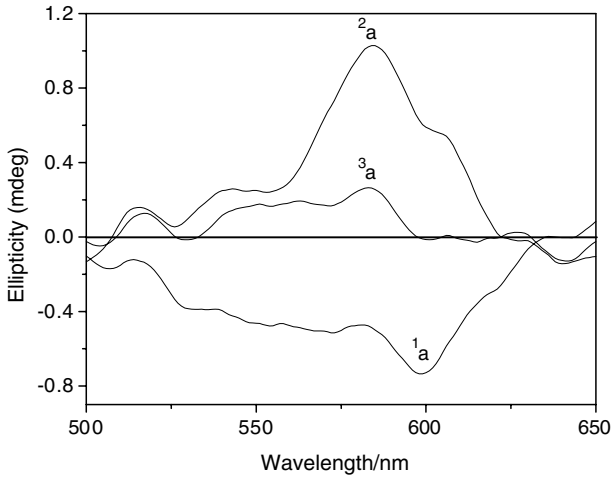

Figure 4. Induced circular dichroism spectra of DNA and compounds **^{1}a**, **^{2}a**, and **^{3}a** at DNA/compound ratio of 10 in Tris–HCl buffer (pH 7.0).

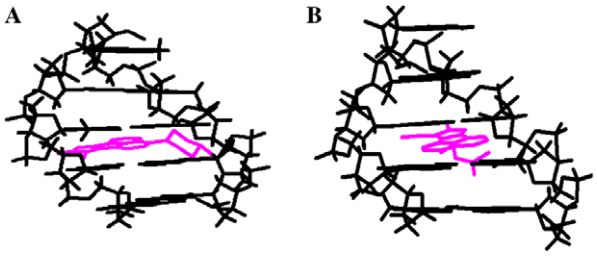

Figure 5. Molecular modeling of **^{1}a**–DNA complex ((A) long axis of **^{1}a** was oriented parallel to the long axis of DNA base pairs) and **^{2}a**–DNA complex ((B) long axis of **^{2}a** was vertical to the long axis of DNA base pairs).

moiety involved much in the binding progress. So the binding affinities of series **I** were lower than those of series **II** and **III**. In addition, the ^{2}**a**–DNA complex showed larger ICD signal than ^{3}**a**–DNA, suggesting that the length of the substitution did affect the intercalation into DNA and short side chain on naphthalene be helpful for intercalation, which was in consistent with the binding affinity results.

2.5. DNA conformational changes

The intrinsic CD spectra of DNA were applied to understand the potential of the present compounds changing the DNA conformation. As shown in Figure 6, the CD spectrum of free CT DNA exhibited a negative band at 244 nm due to the helicity and a positive band at 275 nm due to the base stacking, which was the characteristic of DNA in the right-hand B form.[27,28] When the compounds were incubated with CT DNA, the CD spectrum of DNA underwent changes in both the positive and negative bands (Table 3). The increase of the positive bands and decrease of the negative bands with no significant red shift was observed for all the compounds

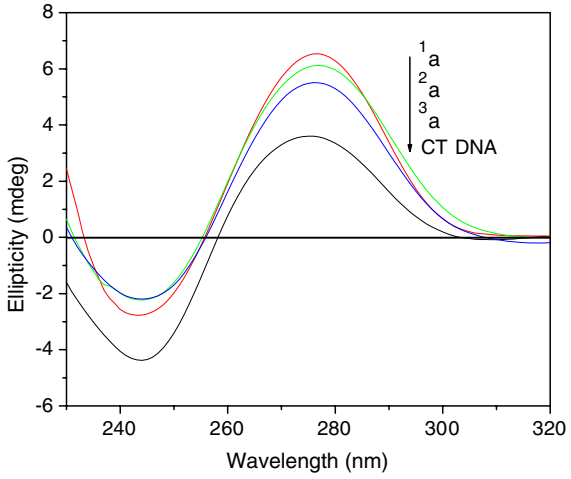

Figure 6. Intrinsic circular dichroism of CT DNA in the absence and presence of compounds ^{1}**a**, ^{2}**a**, and ^{3}**a** at DNA/compound ratio of 5 in Tris–HCl buffer (pH 7.0).

Table 3. CD parameters for the interaction of CT DNA with the compounds

Compound	Molecular ellipticities $[\ominus] \times 10^{-5}$ (deg cm^2 dmol^{-1})	
	Positive band (276 nm)	Negative band (244 nm)
DNA 50 μM	7162	8644
DNA+^{1}**a** 10 μM	13060	5540
DNA+^{1}**b** 10 μM	10708	6420
DNA+^{1}**c** 10 μM	7211	8755
DNA+^{2}**a** 10 μM	12242	4454
DNA+^{2}**b** 10 μM	12094	5966
DNA+^{2}**c** 10 μM	11808	6791
DNA+^{3}**a** 10 μM	11021	4389
DNA+^{3}**b** 10 μM	10943	5847
DNA+^{3}**c** 10 μM	11474	7219

of the three series, which was consistent with the B to A-like conformational change.[29,30] The DNA helical band at 244 nm corresponding to the DNA unwound extent exhibited decrease for all the compounds, with the same orders as that of binding affinity, ^{1}**a** > ^{1}**b** > ^{1}**c**, ^{2}**a** > ^{2}**b** > ^{2}**c**, and ^{3}**a** > ^{3}**b** > ^{3}**c**. Consequently, in each of the three series, the CN-introduced compounds caused the B form DNA to the most unwound form regardless of the substitution.

In particular, it is worth noting that ^{1}**a**, whose binding affinity was one of the lowest, led to the most significant base pair stacking at 275 nm. This may attribute to its intercalation geometry, which was different from that of compounds ^{2}**a** and ^{3}**a**. It was exciting to evaluate ^{1}**a** and other compounds on living species to explore the features that contributed to the biological activity, binding affinity, binding mode, or both.

2.6. Cytotoxicity

The nine compounds were tested for in vitro cytotoxicity against human cervical carcinoma (HeLa) cell line and Human caucasian breast adenocarcinoma (MCF-7) cell line utilizing the MTT assay. All the compounds exhibited outstanding cytotoxic activity with IC_{50} ranging from 10^{-7} to 10^{-6} M[31,32] (Table 4). Compounds ^{1}**c**, ^{2}**c**, and ^{3}**c**, which contain a $COOCH_2CH_2Br$ group in the chromophore, were the strongest growth inhibitors against both the two cell lines. It is acceptable because halogenated hydrocarbons are well-known toxicants.[33,34]

Interestingly, no obvious correlation was found between their DNA binding affinities and antitumor activities. The higher cell killing ability was astoundingly found in the series **I** whose binding affinity was one order of magnitude lower than that of series **II** and **III**. The possible model to account for this behavior involved the different DNA binding geometry between the compounds containing methylpiperazine and alkylamine substitution. One used to believe that for DNA intercalating agents, the main mode of action was potent inhibit of nucleic acid synthesis, which enhanced linearly upon their DNA binding affinity.[10,17] Recently, more and more research revealed that the formation of a ternary complex of DNA, intercalator, and a critical DNA binding protein was much important for the antitumor property, which is related with the binding geometry of ligand–DNA complex.[7,8] So we hypothesized that ^{1}**a** could change the DNA conformation so significantly that the ^{1}**a**–DNA complex might interfere with some critical DNA binding protein. The consequent event of ^{1}**a** intercalating into DNA was, at least partly, the mechanism for its cell killing ability. To this point, the antitumor molecular mechanism of series **I** should be different from that of the series **II** and **III**.

2.7. Compound ^{1}a induced apoptosis in vitro

The mechanism of compounds ^{1}**a**, ^{2}**a**, and ^{3}**a** causing cell death was investigated. Under fluorescence microscope, the live, dead, and apoptotic cells were distinguished clearly through color and morphology by means of

Table 4. Cytotoxicity evaluation of the nine compounds against HeLa and MCF-7 cell line in vitro (IC_{50}, μM)

Compound	^{1}a	^{1}b	^{1}c	^{2}a	^{2}b	^{2}c	^{3}a	^{3}b	^{3}c
HeLa	1.76	2.33	0.79	7.36	8.8	0.72	4.02	8.56	1.38
MCF-7	2.1	1.9	1.1	8.8	8.6	0.33	1.7	9.1	0.44

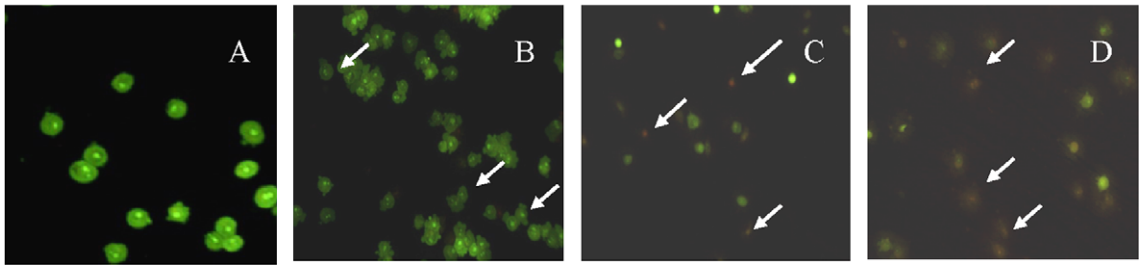

Figure 7. LIVE/DEAD/APOPTOSIS two-color cell viability experiment: (A) untreated MCF-7 cells (live, negative control), (B) cells exposed to 1 μM **^{1}a** for 24 h (cells indicated by arrows are early apoptotic cells), (C) cells exposed to 5 μM **^{1}a** for 24 h (later apoptotic cells), and (D) cells exposed to 5 μM **^{2}a** for 24 h (dead cells).

two-color test. Figure 7 shows **^{1}a** induced MCF-7 cell apoptosis in a dose-dependent manner. After 24 h exposure of 1 μM **^{1}a**, 25.6% cells exhibited apoptosis, most of which were in early phase of apoptosis (green cells whose nuclei present pyknosis), and 12.3% necrotic cell stained as brown cells with nuclear morphology resembling that of viable cells. At this time point, 5 μM **^{1}a** caused 48.3% cell apoptosis, among which cells underwent later cell apoptosis were available (moon-like brown cells whose nuclei present pyknosis), and 23.7% necrotic cells. By contrast, 1 μM **^{2}a** necrotized 22.5% MCF-7 cells, without any significant apoptosis. The similar phenomenon was found for **^{3}a**. As a tightly controlled network of protein–protein interaction, apoptosis was so complicated that multiple protein families were involved. Now it was difficult to assess which protein or factors were interfered with **^{1}a** or **^{1}a**–DNA complex, but it was clear that except for the cytotoxic function which was the same as compounds **^{2}a** and **^{3}a**, **^{1}a** did lead to cell spontaneous programmed death.

In summary, a detailed description of the DNA binding affinity, geometry, and antitumor potential of acenaphtho[1, 2-*b*]pyrrole derivatives was obtained. These series of compounds presented a novel promising platform for the development of antitumor lead compound. In particular, the role of methylpiperazine and alkylamine substitution in both the DNA binding affinity and antitumor property was analyzed. It could be concluded that the binding geometry contributed not only to the binding affinity, but also to the antitumor capacity. In our case, binding geometry contributed much more than binding affinity to the antitumor property of the compounds.

3. Experimental

3.1. Synthesis

All the solvents were of analytical grade. 8-oxo-8*H*-acenaphtho[1,2-*b*]pyrrole-9-carbonitrile and its derivatives were prepared according to our previous report.[35] The synthesis route of 8-oxo-8*H*-acenaphtho[1,2-*b*]pyrrole-9-carboxylic acid methyl ester, 8-oxo-8*H*-acenaphtho[1,2-*b*]pyrrole-9-carboxylic acid-2-bromo-ethyl ester, and their derivatives referred to another previous publication of us.[36] Melting points were determined by an X-6 micro-melting point apparatus (China) and are uncorrected. The ^{1}H NMR spectra were obtained with Bruker AV-400 spectrometer (USA) with chemical shifts reported as ppm (in $CDCl_3$/DMSO-d_6, TMS as internal standard). The IR spectra were measured using a Perkin-Elmer 2000 FTIR instrument (USA). High-resolution mass spectra were obtained on HPLC-Q-Tof MS (Micro) spectrometer (USA). Column chromatography was performed using silica gel 200–300 mesh.

3.1.1. 3-(4-Methyl-piperazin)-8-oxo-8*H*-acenaphtho[1,2-*b*]pyrrole-9-carbonitrile (^{1}**a).** Yield 28%; dark purple solid; mp: 201–202 °C; ^{1}H NMR (400 MHz, $CDCl_3$), δ = 8.68 (d, J = 7.6 Hz, 1H), 8.50 (d, J = 8.4 Hz, 1H), 8.12 (d, J = 8.4 Hz, 1H), 7.82 (dd, J = 8.4, 7.6 Hz, 1H), 7.06 (d, J = 8.4 Hz, 1H), 3.67 (t, J = 4.6 Hz, $N(CH^{*}_2CH_2)_2NCH_3$, 4H), 2.77 (t, J = 4.6 Hz, $N(CH_2CH^{*}_2)_2NCH_3$, 4H), 2.45 ppm (s, NCH_3, 3H). IR (KBr): ν = 3423, 2941, 2214, 1623, 1572 cm^{-1}. HRMS (ESI) *m*/*z*: 329.1415 $[M+H]^+$ (*m*/*z* calcd for $[C_{20}H_{17}N_4O]^+$: 329.1402).

3.1.2. 3-(2-Dimethylamino-ethylamino)-8-oxo-8*H*-acenaphtho[1,2-*b*]pyrrole-9-carbonitrile (^{1}**b).** Yield 38%; dark purple solid; mp: >300 °C; ^{1}H NMR (400 MHz, DMSO-d^6) δ = 8.99 (d, J = 7.6 Hz, 1H), 8.64 (d, J = 7.6 Hz, 1H), 8.02 (d,J = 9.2 Hz, 1H), 7.93 (dd, J = 8.0, 8.0 Hz, 1H), 7.06 (d, J = 9.2 Hz, 1H), 3.79 (br s, $NHCH^{*}_2CH_2$, 2H), 2.93 (br s, $NHCH_2CH^{*}_2$, 2H), 2.44 ppm (s, $N(CH_3)_2$, 6H). IR (KBr): ν = 2949, 2212, 1631, 1577, 1526 cm^{-1}. HRMS (ESI) *m*/*z*: 343.1557 $[M+H]^+$ (*m*/*z* calcd for $[C_{19}H_{17}N_4O]^+$: 343.1559).

3.1.3. 3-(3-Dimethylamino-propylamino)-8-oxo-8*H*-acenaphtho[1,2-*b*]pyrrole-9-carbonitrile (^{1}**c).** Yield 38%; dark purple solid; mp: > 300 °C; ^{1}H NMR (400 MHz, DMSO-d^6) δ = 8.86 (d, J = 8.0 Hz, 1H), 8.58 (d,

J = 7.6 Hz, 1H), 7.95 (d, J = 9.2 Hz, 1H), 7.90 (dd, J = 8.0, 7.6 Hz, 1H), 7.02 (d, J = 9.2 Hz, 1H), 3.65 (t, J = 6.7, 7.1 Hz, NHCH^*_2CH$_2$, 2H), 3.28 (m, CH^*_2N(CH$_3$)$_2$, 2H), 2.30 (s, N(CH$_3$)$_2$, 6H), 1.92 ppm (m, CH$_2$, 2H). IR (KBr): v = 2927, 2821, 2202, 1625, 1572, 1535 cm^{-1}. HRMS (ESI) m/z: 329.1409 [M−H]$^-$ (m/z calcd for [C$_{20}$H$_{17}$N$_4$O]$^-$: 329.1402).

3.1.4. 3-(4-Methyl-piperazin)-8-oxo-8*H*-acenaphtho[1,2-*b*]pyrrole-9-carboxylic acid methyl ester (^{2}a). Yield 32%; dark purple solid; mp: 210 °C dec; ^{1}H NMR (400 MHz, CDCl$_3$): δ = 9.01 (d, J = 8.0 Hz, 1H), 8.77 (d, J = 7.6 Hz, 1H), 8.46 (d, J = 8.4 Hz, 1H), 7.78 (dd, J = 8.0, 7.6 Hz, 1H), 7.17 (d, J = 8.4 Hz, 1H), 3.55 (br s, N(CH^*_2CH$_2$)$_2$NCH$_3$, 4H), 3.17 (s, COOCH^*_3, 3H), 3.46 (br s, N(CH$_2$ CH^*_2)$_2$NCH$_3$, 4H), 2.48 ppm (br s, NCH$_3$, 3H). IR (KBr): v = 2929, 1765, 1702, 1629, 1572, 1509 cm^{-1}. HRMS (ESI) m/z: 362.1449 [M+H]$^+$ (m/z calcd for [C$_{21}$H$_{20}$N$_3$O$_3$]$^+$: 362.1505).

3.1.5. 3-(Dimethylamino-ethylamino)-8-oxo-8*H*-acenaphtho[1,2-*b*]pyrrole-9-carboxylic acid methyl ester (^{2}b). Yield 38%; dark purple solid ; mp: 220 °C dec; ^{1}H NMR (400 MHz, DMSO-d^6): δ = 8.84 (d, J = 8.8 Hz, 2H), 8.62 (d, J = 7.2 Hz, 1H), 7.85 (dd, J = 7.2, 8.0 Hz,1H), 7.02 (d, J = 8.8 Hz, 1H), 3.71 (br s, NHCH^*_2CH$_2$, 2H), 2.98 (s, COOCH$_3$, 3H), 2.84 (br s, 2H, CH^*_2N(CH$_3$)$_2$), 2.41 ppm (s, CH$_2$N(CH^*_3)$_2$, 6H). IR (KBr): v = 2923, 1765, 1703, 1685, 1654, 1626, 1563 cm^{-1}; HRMS (ESI) m/z: 350.1505 [M+H]$^+$ (m/z calcd for [C$_{20}$H$_{20}$N$_3$O$_3$]$^+$: 350.1505).

3.1.6. 3-(Dimethylamino-propylamino)-8-oxo-8*H*-acenaphtho[1,2-*b*]pyrrole-9-carboxylic acid methyl ester (^{2}c). Yield 35%; dark purple solid; mp: 186–187 °C; ^{1}H NMR (400 MHz, DMSO-d^6): δ = 8.79 (d, J = 8.8 Hz, 2H), 8.59 (d, J = 7.6 Hz, 1H), 7.84 (dd, J = 7.6, 8.0 Hz, 1H), 6.99 (d, J = 8.8 Hz, 1H), 3.61 (br s, NHCH^*_2CH$_2$, 2H), 3.17 (br s, (CH$_3$)$_2$NCH^*_2CH$_2$, 2H), 2.98 (s, COOCH$_3$, 3H), 2.38 (s, N(CH$_3$)$_2$, 6H), 1.95 ppm (m, NHCH$_2$CH^*_2, 2H). IR (KBr): v = 3047, 2912, 1749, 1702, 1624, 1567, 1545, 1511 cm^{-1}. HRMS (ESI) m/z: 364.1665 [M+H]$^+$ (m/z calcd for [C$_{21}$H$_{22}$N$_3$O$_3$]$^+$: 364.1661).

3.1.7. 3-(4-Methyl-piperazin-1-yl)-8-oxo-8*H*-acenaphtho[1,2-*b*]pyrrole-9-carboxylic acid 2-bromo-ethyl ester (^{3}a). Yield 26%; dark purple solid; mp: 220 °C dec; ^{1}H NMR (500 MHz, DMSO-d^6): δ = 8.97 (d, J = 8.0 Hz, 1H), 8.65 (d, J = 7.6 Hz, 1H), 8.61 (d, J = 8.4 Hz, 1H), 7.94 (dd, J = 8.0, 7.6 Hz, 1H), 7.47 (d, J = 8.4 Hz, 1H), 4.13 (t, J = 6.4 Hz, OCH$_2$, 2H), 3.72 (t, J = 6.4 Hz, CH$_2$Br, 2H), 3.55 (br s, N(CH^*_2CH$_2$)$_2$NCH$_3$, 4H), 3.46 (br s, N(CH$_2$ CH^*_2)$_2$NCH$_3$, 4H), 2.49 ppm (br s, NCH$_3$, 3H). IR (KBr): v = 2929, 1765, 1702, 1629, 1572, 1509 cm^{-1}. HRMS (EI) m/z: 453.0692 [M$^\cdot$] (m/z calcd for [C$_{22}$H$_{20}$BrN$_3$O$_3^\cdot$] 453.0688).

3.1.8. 3-(Dimethylamino-ethylamino)-8-oxo-8*H*-acenaphtho[1,2-*b*]pyrrole-9-carboxylic acid 2-bromo-ethyl ester (^{3}b). Yield 35%; dark purple solid; mp: >300 °C; ^{1}H NMR (400 MHz, DMSO-d^6): δ = 8.85 (d, J = 8.0 Hz, 1H), 8.78 (d, J = 8.8 Hz, 1H), 8.60 (d, J = 7.2 Hz, 1H), 7.85 (dd, J = 7.2, 8.0 Hz, 1H), 7.03 (d, J = 8.8 Hz, 1H), 3.92 (t, J = 6.4 Hz, OCH^*_2, 2H), 3.71 (t, J = 6.4 Hz, CH$_2$Br, 2H), 3.69 (t, J = 6.4 Hz, NHCH^*_2, 2H), 2.69 (t, J = 6.4 Hz, CH^*_2N(CH$_3$)$_2$, 2H), 2.29 ppm (s, N(CH$_3$)$_2$, 6H). IR (KBr): v = 2928, 1750, 1698, 1625, 1572, 1546 cm^{-1}. HRMS (ESI) m/z: 442.0753 [M+H]$^+$ (m/z calcd for [C$_{21}$H$_{21}$BrN$_3$O$_3$]$^+$: 442.0766).

3.1.9. 3-(Dimethylamino-propylamino)-8-oxo-8*H*-acenaphtho[1,2-*b*]pyrrole-9-carboxylic acid 2-bromo-ethyl ester (^{3}c). Yield 32%; dark purple solid; mp: 220 °C dec; ^{1}H NMR (400 MHz, DMSO-d^6): δ = 9.52 (br s, NH), 8.84 (d, J = 8.0 Hz, 1H), 8.83 (d, J = 8.8 Hz, 1H), 8.63 (d, J = 7.6 Hz, 1H), 7.88 (dd, J = 7.6, 8.0 Hz, 1H), 7.05 (d, J = 8.8 Hz, 1H), 3.93 (t, J = 6.4 Hz, OCH$_2$, 2H), 3.71 (t, J = 6.4 Hz, CH$_2$Br, 2H), 3.63 (br s, 2H, NHCH^*_2), 2.67 (br s, CH^*_2N(CH$_3$)$_2$,2H), 2.40 (s, N(CH$_3$)$_2$, 6H), 1.96 ppm (m, CH$_2$CH^*_2CH$_2$, 2H). IR (KBr): v = 2938, 2776, 1748, 1698, 1626, 1571, 1546, 1507 cm^{-1}. HRMS (ESI) m/z: 456.0930 [M+H]$^+$ (m/z calcd for [C$_{22}$H$_{24}$BrN$_3$O$_3$]$^+$: 456.0923).

3.2. DNA binding studies

3.2.1. Materials. SYBR Green was purchased from The Molecular Probes Company (USA). Tris Base was from Promega Company (USA). Calf thymus DNA (CT DNA) was obtained from Sigma Chemical Company (USA). Stock of CT DNA was prepared by dissolving commercial nucleic acids in Tris–HCl buffer at pH 7.0 and stored at 4 °C for more than 24 h to get homogeneity. The concentration of CT DNA was determined spectrophotometrically from the molar absorption coefficient (6600 M^{-1} cm^{-1}) at 260 nm as well as its purity checked by the absorbance ratio A_{260}/A_{280} that should not be less than 1.8.[37] Doubly purified water used in all experiment was from MILLI-Q system. All the chemicals and solvents were of reagent grade and used without further purification.

3.2.2. DNA binding affinity. SYBR Green–DNA melt curve was recorded on SmartCycler **II** (TaKaRa, USA). The contrast was obtained by incubating 1:5000 dilution SYBR Green with CT DNA (50 μM) for 15 min. Each compound (10 μM) was added into the former mixture then samples were transferred to SmartCycler tube and heated from 45 to 95 °C. Fluorescence intensities were recorded as SYBR Green–DNA melt curve.

The fluorescence spectra were scanned with a FP-6500 spectrophotometer (Jasco, Japan) at room temperature in a 1-cm quartz cuvette. Titrations were performed by keeping the DNA concentration as 50 μM while varying the compound concentration from 1 to 10 μM. Fluorescence intensity was recorded after each addition of DNA. The difference in fluorescence intensity of the compounds in the absence and presence of DNA (fluorescence quenching) was assumed to be proportional to the amount of DNA-bound compound. The binding affinity (K_b) and binding intensity n were calculated.[38]

3.2.3. Absorption titration. The absorption titrations were performed using a HP 8453 spectrophotometer (HP, USA). A 1-cm path quartz cell was used for the

measurement. The titration absorption spectra of compound by CT DNA were measured by keeping the compound concentration at 10 μM while varying the DNA concentration from 5 to 50 μM (at 5 μM intervals).

3.2.4. Circular dichroism spectra. Circular dichroism spectra were scanned with a J-810 spectrophotometer (Jasco, Japan) using a 1-cm path quartz cell and subtracted from the spectrum of buffer alone. The induced circular dichroism spectra were scanned in the range of 450 ~ 700 nm for the compound–DNA complex at DNA/compound ratio of 10 and the intrinsic circular dichroism spectra in 230 ~ 320 nm were recorded for DNA at DNA/compound ratio of 5.

3.3. Cytotoxicity experiments

HeLa cell line and MCF-7 cell line were obtained from China Center for Type Culture Collection (Wuhan, China). Cells were cultured in 75 cm^2 Falcon flasks (Becton–Dickinson, Franklin Lakes) in phenol-red-free RPMI medium 1640 (Gibco/BRL) supplemented with fetal calf serum (10%), Hepes (10 mM), sodium bicarbonate (24 mM), sodium pyruvate (1 mM), 2-mercaptoethanol (0.05 μM), penicillin (60 μg/mL), and streptomycin (100 μg/mL). Cell culture was kept in a humidified incubator with 5% CO_2 at 37 °C. Then cells were seeded into 24-well (1×10^4 cells per well) plates. After cells were cultured in the presence of various concentrations of compound (0.01–100 μM) from DMSO stock (1–10 mM) for 24 h, medium was aspirated and replenished with complete medium. IC_{50} was evaluated by metabolite 3-[4, 5-dimethylthiazol- 2-yl]-2, 5-diphentetrazolium bromide (MTT) metabolic labeling assay.[39] Each experiment was performed three times.

3.4. Assessment of apoptosis

MCF-7 cells were cultured as above. Twenty-four hours after 1 and 5 μM **^{1}a**, **^{2}a**, and **^{3}a** exposure, the cells were harvested and stained by LIVE/DEAD/APOPTOSIS detection kit according to the protocol provided with the kit (Keygen Biotech. Co. Ltd, China). Fluorescence microscopy images were taken by a Nikon fluorescence microscope (TE2000, Japan) equipped with a real-time video camera and a standard fluorescence excitation filter set. For every sample, apoptotic cells or dead cells were counted in randomly selected, noncontiguous, ×200 microscopic fields.

Acknowledgment

This work was supported by the National Natural Science Foundation of China.

References and notes

1. Wang, L.; Price, H. L.; Juusola, J.; Kline, M.; Phanstiel, O., IV *J. Med. Chem.* **2001**, *44*, 3682.
2. Braña, M. F.; Cacho, M.; Carcía, M. A.; Pascual-Teresa, B.; Ramos, A.; Acero, N.; Llinares, F.; Muñoz-Mingarro, D.; Abradelo, C.; Rey-Stolle, M. F.; Yuste, M. *J. Med. Chem.* **2002**, *45*, 5813.
3. Lee, Y.-A.; Lee, S.; Cho, T.-S.; Kim, C.; Han, S. W.; Kin, S. K. *J. Phys. Chem. B* **2002**, *106*, 11351.
4. Haq, I.; Lincoln, P.; Suh, D.; Nordén, B. *J. Am. Chem. Soc.* **1995**, *117*, 4788.
5. Eriksson, M.; Leijon, M.; Hiort, C.; Nordén, B.; Gräslund, A. *Biochemistry* **1994**, *33*, 5031.
6. Viola, G.; Acqua, F. D.; Gabellini, N.; Moro, S.; Vedaldi, D.; Ihmels, H. *Chem. BioChem.* **2002**, *3*, 550.
7. Cholody, W. M.; Kosakowka-Cholody, T.; Hollingshead, M. G.; Hairprakasha, H. K.; Michejda, C. J. *J. Med. Chem.* **2005**, *48*, 4474.
8. Tarasov, S. G.; Casas-Finet, J. R.; Cholody, W. M.; Kosakowka-Cholody, T.; Gryzynski, Z. K.; Michejda, C. J. *Photochem. Photobiol.* **2003**, *78*, 313.
9. Catoen-Chackal, S.; Facompre, M.; Houssin, R.; Pommery, N.; Goossens, J.-F.; Colson, P.; Bailly, C.; Hénichart, J.-P. *J. Med. Chem.* **2004**, *47*, 3665.
10. Xu, Y.; Qu, B.; Qian, X.; Li, Y. *Bioorg. Med. Chem. Lett.* **2005**, *15*, 1139.
11. Rescifina, A.; Chiacchio, M. A.; Corsaro, A.; Clercq, E. D.; Iannazzo, D.; Mastino, A.; Piperno, A.; Romeo, G.; Romeo, R.; Valveri, V. *J. Med. Chem.* **2006**, *49*, 709.
12. Bolognese, A.; Correale, G.; Manfra, M.; Lavecchia, A.; Mazzoni, O.; Novellino, E.; Barone, V.; Colla, P. L.; Loddo, R. . *J. Med. Chem* **2002**, *45*, 5217.
13. Zhang, Z.; Yang, Y.; Liu, F.; Qian, X.; Xu, Q. *Int. J. Biol. Macromol.* **2006**, *38*, 59.
14. Zhang, Z.; Lu, Z.; Qian, X.; Liu, F.; Sheng, H. *Chem. Res. Chin. U.* **2005**, *21*, 480.
15. Walton, T. A.; Lyttle, M. H.; Dick, D. J.; Cook, R. M. *Bioconjug. Chem.* **2002**, *13*, 1155.
16. Jobs, M.; Fredriksson, S.; Brookes, J. A.; Landegren, U. *Anal. Chem.* **2002**, *74*, 199.
17. Kumar, C. V.; Punzalan, E. H. A.; Tan, W. B. *Tetrahedron* **2000**, *56*, 7027.
18. Xiao, S.; Lin, W.; Wang, C.; Yang, M. *Bioorg. Med. Chem. Lett.* **2001**, *11*, 437.
19. Modukuru, N. K.; Snow, K. J.; Perrin, B. S.; Thota, Jr. J.; Kumar, C. V. *J. Phys. Chem. B* **2005**, *109*, 11810.
20. Selvi, P. T.; Palaniandavar, M. *Inorg. Chim. Acta* **2002**, *337*, 420.
21. Hörmann, A.; Chaudhuri, B.; Fretz, H. *Bioorg. Med. Chem.* **2001**, *9*, 917.
22. Juskowiak, B.; Galęzowska, E.; Takenaka, S. *Spectrochim. Acta A* **2003**, *59*, 1083.
23. Lyng, R.; Härd, T.; Nordén, B. *Biopolymers* **1987**, *26*, 1327.
24. Lyng, R.; Rodger, A.; Nodén, B. *Bioploymers* **1991**, *31*, 1709.
25. Becker, H.-C.; Nodén, B. *J. Am. Chem. Soc.* **1999**, *121*, 11947.
26. Becker, H.-C.; Nodén, B. *J. Am. Chem. Soc.* **1997**, *119*, 5798.
27. Jiang, X.; Shang, L.; Wang, Z.; Dong, S. *Biophys. Chem.* **2005**, *118*, 42.
28. Maheswari, P. U.; Palaniandavar, M. *Inorg. Chim. Acta* **2004**, *357*, 901.
29. Nikolis, N.; Methenitis, C.; Pneumatikakis, G. *J. Inorg. Biochem.* **2003**, *95*, 177.
30. Maheswari, P. U.; Palaniandavar, M. *J. Inorg. Biochem.* **2004**, *98*, 219.
31. Viktor, G.; Manuel, H. *J. Natl. Cancer Inst.* **2003**, *95*, 851.
32. Sami, S. M.; Dorr, R. T.; Solyom, A. M.; Alberts, D. S.; Remers, W. A. *J. Med. Chem.* **1995**, *38*, 983.
33. Hammond, A. H.; Garle, M. J.; Fry, J. R. *Toxicol. Appl. Pharmcol.* **1999**, *155*, 287.

34. Parra-Delgado, H.; Ramírez-Apan, T.; Martínez-Vázquez, M. *Bioorg. Med. Chem.* **2005**, *15*, 1005.
35. Liu, F.; Xiao, Y.; Qian, X.; Zhang, Z.; Cui, J.; Cui, D.; Zhang, R. *Tetrahedron* **2005**, *61*, 11264.
36. Liu, F.; Qian, X.; Cui, J.; Xiao, Y.; Zhang, R.; Li, G. *Bioorg. Med. Chem.* **2006**, *13*, 4639.
37. Huang, W.; Zhang, Z.; Han, X.; Tang, J.; Wang, J.; Dong, S.; Wang, E. *Bioelectrochemistry* **2003**, *59*, 21.
38. Gupta, M.; Ali, R. *J. biochem.* **1984**, *95*, 1253.
39. Wu, S. P.; Sun, L. Z.; Willson, J. V. K.; Humphrey, L.; Kerbel, R.; Brat-tain, M. G. *Cell Growth Differ.* **1993**, *4*, 115.